

BENDING BEHAVIOUR OF GLT-STEEL BEAM CONNECTED BY INCLINED SCREWS

Sung-Jun Pang¹, Kyung-Sun Ahn², Gwang-Ryul Lee³, Min-Jeong Kim⁴,
Jae-Won Oh⁵, Jung-Kwon Oh⁶

ABSTRACT: In this study, a glued-laminated timber (GLT) was reinforced with a steel plate and inclined screws, and its bending performance was analyzed. In a total of 8 GLTs, 3 GLTs were not reinforced (control group) and 5 GLTs were reinforced with steel plates (comparison group). The size of GLT was 80 mm (width) × 120 mm (thickness) × 2400 mm (length). The GLT in the comparison group, a steel plate (SPHC-P, yield strength: 227 MPa, modulus of elasticity 166.33 GPa) was installed with screws (Ø9x160mm, 45°). The deflection and load of specimens were measured by a third-point bending test to derive their bending stiffness and load-carrying capacities. As a result of the experiment, all specimens in the control group showed brittle tensile failure, but all specimens of the comparison group showed ductile behavior and maintained a load-bearing capacity of about 30 kN. After the compression failure of the GLT, there was no damage to the screw connection while the steel plate was extended. Therefore, the screw connection sufficiently supported the shear force generated between GLT and steel plate, and the steel plate reinforcement completely changed the GLT behavior.

KEYWORDS: Glued-laminated timber (GLT), Steel, Screw, Beam, Bending behavior

1 INTRODUCTION

Glued-laminated timber (GLT) and steel are structural building materials used in dry construction and recyclable. Both materials are cut or drilled in the factory using CNC cutting machines, so the machining precision is high and the machining error is small.

Several hybrid beams have been developed with GLT and steels. When the GLT are reinforced by steel, the bending performance of the GLT beam is improved and the deviation is reduced (André, Alan, 2006). Generally, the two materials are glued with an adhesive, but it is not easy to maintain the adhesive performance enough to resist a large external force.

In this study, a new GLT and steel composite beam was designed which were mechanically joined using screws instead of bonding. The bending performance and failure modes of the mechanically connected GLT and steel beams were analyzed.

2 MATERIALS AND METHODS

2.1 SPECIMENS

Figure 1 shows the cross section of GLT and the combination of lamina. One lamina grade (E9) was used, and the modulus of elasticity (MOE) of that grade was greater than 9 GPa. The size of GLT was 80 mm (width) × 120 mm (thickness) × 2400 mm (length).

For GLT-steel beam specimens, a steel plate (SPHC-P, yield strength: 227 MPa, modulus of elasticity 166.33 GPa) was installed with screws (Ø9x160mm, 45°).

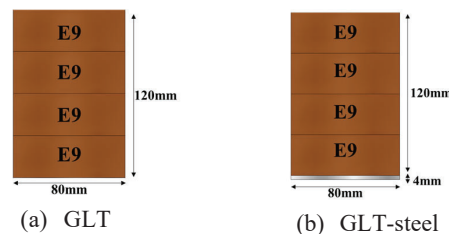


Figure 1: Cross section of GLT and GLT-steel specimen

¹ Department of Agriculture, Forestry and Bioresources, Seoul National University, Republic of Korea, pangsungjun@snu.ac.kr

² Department of Agriculture, Forestry and Bioresources, Seoul National University, Republic of Korea, rudtjs6339@snu.ac.kr

³ Department of Agriculture, Forestry and Bioresources, Seoul National University, Republic of Korea, qweqweqwer@snu.ac.kr

⁴ Department of Agriculture, Forestry and Bioresources, Seoul National University, Republic of Korea, minjeong.kim@snu.ac.kr

⁵ Department of Agriculture, Forestry and Bioresources, Seoul National University, Republic of Korea, redhurse@snu.ac.kr

⁶ Department of Agriculture, Forestry and Bioresources, Seoul National University, Republic of Korea, jungoh@snu.ac.kr

2.2 BENDING TEST

The deflection and load resistance of specimens were measured by a third-point bending test to derive their bending stiffness and load-carrying capacities (Figure 2).

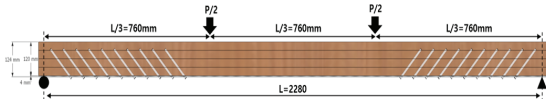


Figure 2: Cross section of GLT and GLT-steel specimen

Figure 3 shows the total thickness, neutral axis, and maximum load resistance of the specimen according to the thickness of the steel plate reinforcing the GLT. When GLT was reinforced with a steel thickness of 3 mm or less, the maximum load of the beam was governed by the tensile failure of the steel plate. However, when GLT was reinforced with a steel thickness of 4 mm or more, the maximum load of the beam was governed by compression failure of wood. Thus, in this study, when GLT was reinforced with a 4mm thick steel plate, it was checked whether or not compression failure of wood occurred.

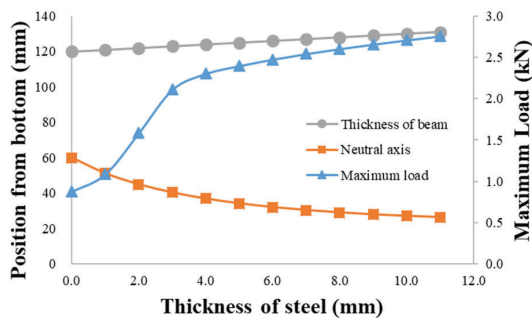


Figure 3: Thickness of beam, neutral axis, and maximum load resistance by steel plate thickness

3 RESULTS AND DISCUSSION

Figure 4 shows the failure mode of the non-reinforced GLT specimen. All specimens were broken around the knot in the tensile zone. At the time of failure, the load resistance dropped sharply as shown in Fig. 5. This brittle failure is a typical failure mode of GLT or wood in bending tests.

In the case of non-reinforced GLT, the bending stiffness was about 0.16×10^{12} N/mm² and the maximum load was 28.2 kN, which was determined by brittle failure.

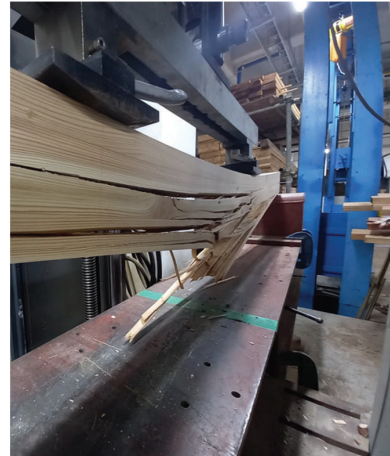


Figure 4: Failure mode of the non-reinforced GLT specimens

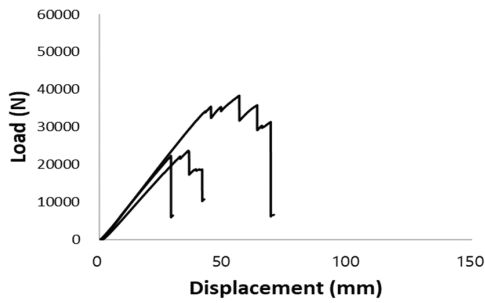


Figure 5: Load-displacement curve of the non-reinforced GLT specimens (three specimens)

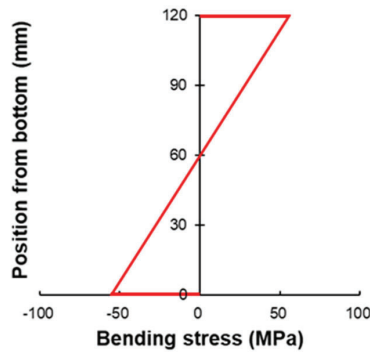


Figure 6: Bending stress distribution of non-reinforced GLT specimens at the maximum bending moment

Figures 7 through 9 show the failure mechanism of the reinforced GLT specimens. In two of the five specimens, tensile failure occurred first at the finger joint (Fig. 7a) or knot (Fig. 8a) of GLT. The finger-joint and knots are the main factors causing the strength reduction (Pang et al. 2011, 2018, 2021; Pang and Jeong 2019). Unlike the non-reinforced GLT, compression failure occurred at the top of the GLT (Fig. 7b and Fig. 8b) and large deformation occurred (Fig. 7c and Fig. 8c).

In three of the five specimens, compressive failure occurred first at the top of the GLT (Fig. 9a). After that, tensile failure occurred at the knot, but the tensile failure of the specimens did not lead to rapid brittle failure. The specimens showed ductile behavior due to the elongation of the steel plate. The elongation of the steel plate shows that the screw connection sufficiently supported the shear force between GLT and the steel plate.



(a) Tensile failure at finger joint of GLT



(b) Compression failure on top of GLT



(c) Tensile Large deformation

Figure 7: Fracture mechanism of reinforced GLT in which tension failure (finger joint) of GLT occurs first



(a) Tensile failure at knot of GLT



(b) Compression failure on top of GLT



(c) Large deformation

Figure 8: Fracture mechanism of reinforced GLT in which tension failure (knot) of GLT occurs first



(a) Compression failure on top of GLT



(b) Tension failure on bottom of GLT



(c) Large deformation

Figure 9: Fracture mechanism of reinforced GLT in which compression failure of GLT occurs first

Figure 10 shows the load-displacement curve of the reinforced GLT specimens. Unlike the non-reinforced GLT, the reinforced GLT did not lose its load-carrying capacity significantly after the initial failure and maintained a load-carrying capacity of approximately 30 kN. The maximum load-carrying capacity was higher in the case where the compression failure occurred first (48 kN to 51 kN) than in the case where the tensile failure occurred first (32 to 38 kN). This shows that the tensile part (bottom of GLT) contributes to the load-carrying capacity of the reinforced GLT until the tensile failure occurred. The bending stiffness was also improved by about 64% from 0.161 to 0.265×10^{12} N/mm² by the reinforcement, and the coefficient of variation decreased from 0.056 to 0.03.

There was no screw damage while the steel was extending. This means that the screw connection supported the shear force generated between the wood and the steel plate.

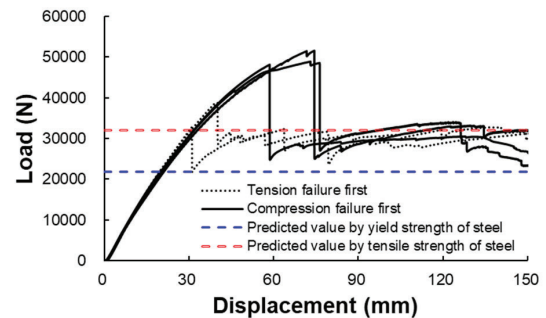


Figure 10: Load-displacement curve of the GLT specimens reinforced with a 4mm thick steel plate (five specimens)

As mentioned above, the reinforced GLT beam continuously supported a load of about 30 kN while undergoing large deformation. Figure 11 shows the bending stress distribution of reinforced GLT by elastic analysis (Eq. 1). The maximum bending stress acting on the steel plate (466.3 MPa, Fig. 11(a)) exceeds the yield strength of the used steel plate (227 MPa). This means that the steel plate was in a plastic state, and plastic analysis is required.

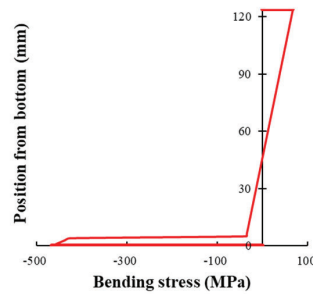
$$\sigma_{bending} = E_i \cdot \varepsilon_i \quad (1)$$

where $\sigma_{bending}$ is the bending stress in the elastic analysis (MPa), E_i is the elastic modulus of i material (MPa), and ε_i is the strain of i material.

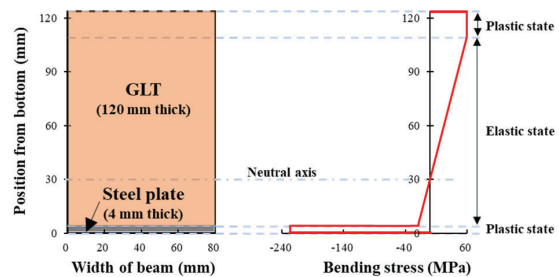
Figure 11(b) shows the bending stress distribution of reinforced GLT considering the plasticity of the GLT and steel. The maximum bending moment of the reinforced GLT can be predicted by Eq. 2. Equation 2 consists of three terms. The first term is the plastic bending moment in GLT, the second term is the elastic bending moment in GLT, and the third term is the plastic bending moment of the steel plate. In the compression test of wood, the load-displacement curve shows a ductile behavior in which the strength decreases slowly as the wood wrinkles after the maximum load (Pang and Jeong 2018). For plastic analysis of reinforced GLT, the load-displacement curve of GLT in compressive stress was idealized as an elastic-plastic curve. Among the reported experimental data (Pang and Jeong 2018; Park *et al.* 2010), the compressive strength (58.8 MPa) of wood with similar elastic modulus in the same species was regarded as the yield strength of GLT,

$$M_{max} = \int_{c_1-h_{c,GLT}}^{c_1} \sigma_{c,GLT} \cdot y \, dA + \int_{c_2-t_{steel}}^{c_1-h_{c,GLT}} E_{GLT} \cdot \varepsilon_{GLT} \cdot y \, dA + \int_{c_2-t_{steel}}^{c_2} f_y \cdot y \, dA \quad (2)$$

where M_{max} is the maximum bending moment (kN·m), c_1 is the distance between the top surface and the neutral axis of the composite section (mm), $h_{c,GLT}$ is the height of the compressive zone in GLT (mm), $\sigma_{c,GLT}$ is the compressive strength of GLT (MPa), y is the distance from the neutral axis of the composite section (mm), c_2 is the distance between the bottom surface and the neutral axis of the composite section (mm), t_{steel} is the thickness of steel plate (mm), E_{GLT} is the elastic modulus of GLT (MPa), ε_{GLT} is the strain of GLT, and f_y is the yield strength of steel plate (MPa).



(a) Elastic analysis (bending stress exceeds the yield strength (227 MPa) of the steel)



(b) Elastic-plastic analysis

Figure 11: Bending stress distribution of the reinforced GLT specimen at the maximum bending moment

Figure 12 shows the bending stress distribution of the reinforced GLT when the steel and timber in compressive zone reach plastic state. The compressive force acting on the upper part of the GLT and the tensile force by the steel plate are equal. Thus, the height of the compressive zone in the reinforced GLT can be calculated by Eq. 3. Figures 12 (a) and (b) show when the maximum stress of steel reached the yield strength (227 MPa) and the tensile strength (345 MPa) of the steel plate, respectively. When the maximum stress of the steel from yield strength to maximum tensile strength increased the height of the compressive zone in the reinforced GLT also increased.

The bending moment and the load-carrying capacity of the reinforced GLT can be predicted by Eq. 4, and Eq. 5, respectively. The predicted load-carrying capacity of reinforced GLT was 21,845 N by applying yield strength of steel (227 MPa) and 32,035 N by applying yield strength of steel (345 MPa). Figure 10 shows the load-carrying capacity predicted by Eq. 5 together with the experimentally measured load-displacement curve. The load capacity predicted by the tensile strength of the steel was similar to the maximum load capacities at the plastic condition of the test specimens. This indicates that the steel plate almost reached its maximum tensile strength. In addition, all of the load capacities of the test specimens were higher than the load predicted by the yield strength of steel. Therefore, the bending moment of GLT reinforced by steel plate can be safely designed with the yield strength of steel.

$$h_{c,GLT} = \frac{f_y \cdot t_{steel}}{\sigma_{c,GLT}} \quad (3)$$

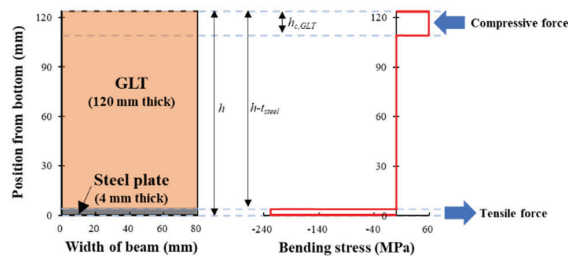
$h_{c,GLT}$ is the the height of the compressive zone in GLT (mm), f_y is the yield or tensile strength of steel plate (MPa), t_{steel} is the thickness of steel plate (MPa), and $\sigma_{c,GLT}$ is the compressive strength of GLT (MPa).

$$M_{predict} = f_y \cdot w \cdot t_{steel} \cdot \left(h - \frac{t_{steel}}{2} - \frac{h_{c,GLT}}{2} \right) \quad (4)$$

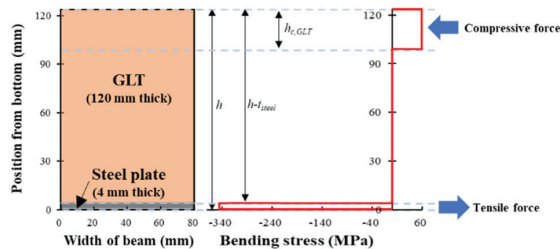
where $M_{predict}$ is the predicted bending moment (kN·m), f_y is the yield or tensile strength of steel plate (MPa), w is the width of steel plate (mm), t_{steel} is the thickness of steel plate (mm), h is the height of reinforced GLT (mm), and $h_{c,GLT}$ is the height of compressive zone in GLT (mm).

$$P_{predict} = \frac{M_{predict}}{L_e} \cdot 2 \quad (5)$$

where $P_{predict}$ is the predicted load-carrying capacity of reinforced GLT (kN), $M_{predict}$ is the predicted bending moment (kN·m), and L_e is the the distance between the load position and support position (mm).



(a) Bending stress distribution at the yield strength (227 MPa) of the steel plate



(a) Bending stress distribution at the tensile strength (345 MPa) of the steel plate

Figure 12: Bending stress distribution of the reinforced GLT specimens at the plastic state

4 CONCLUSIONS

1. The load resistance of non-reinforced GLT decreased to zero after brittle failure in the tensile side of the GLT. However, the reinforced GLT specimen showed ductile behavior even after GLT failure and maintained a load resistance of about 30 kN during

large deformation. The bending stiffness was also improved by about 64% from 0.161 to 0.265 by the reinforcement.

2. The prediction model for the load-carrying capacity of the reinforced GLT was developed based on the compressive strength of wood and the yield strength of steel. The experimentally measured load capacity of the beam was higher than the load predicted load capacity. Therefore, the load and bending moment of the reinforced GLT can be designed with the compressive strength of wood and yield strength of steel.
3. The GLT and steel plate were mechanically connected using only inclined screws without the use of any adhesives. The resistance of the screw sufficiently supported the shear forces so that the steel plate can perform plastic behavior after yielding. This study shows the possibility of non-adhesive composite beam, and additional research to optimize the mechanical connection is needed.

ACKNOWLEDGEMENT

This research was supported by Basic Science Research Program through the National Research Foundation of Korea (NRF) funded by the Ministry of Education (No. NRF-2021R111A1A01045628).

REFERENCES

- André, A. (2006). "Fibres for Strengthening of Timber Structures," *Master Thesis, Luleå tekniska universitet, Civil and Environmental Engineering, Structural Engineering*.
- ASTM D198-15 (2010). "Standard test methods of static tests of lumber in structural sizes," ASTM International, West Conshohosken, PA, USA .
- BS EN 408:2010+A1:2012 (2012). "Timber structures - Structural timber and glued laminated timber - Determination of some physical and mechanical properties," British Standards Institution, London.
- Chang-Min, S., and Hyun-Chul, J. (2009). "Structural analysis of S-cam brake shoe for commercial vehicle by FEM," *J. Ocean Eng. Technol.* 23(4), 69-77.
- Dietsch, P., and Brandner, R. (2015). "Self-tapping screws and threaded rods as reinforcement for structural timber elements - A state-of-the-art report," *Construction and Building Materials* 97, 78-89. DOI: 10.1016/j.conbuildmat.2015.04.028
- ETA-11/0030. (2019). "European technical assessment. Screws for use in timber construction. ETA-Denmark, Nordhavn," ETA-11/0030. (2019). European technical assessment. Screws for use in timber construction. ETA-Denmark, Nordhavn.
- Gerilla, G. P., Teknomo, K., and Hokao, K. (2007). "An environmental assessment of wood and steel reinforced concrete housing construction," *Building and Environment*, 42(7), 2778-2784. DOI: 10.1016/j.buildenv.2006.07.021
- Hafner, A., and Schäfer, S. (2018). "Environmental

- aspects of material efficiency versus carbon storage in timber buildings,” *European Journal of Wood and Wood Products*, 76(3), 1045-1059. DOI: 10.1007/s00107-017-1273-9
- KS D3501 (2018). “Hot-rolled mild steel plates, sheets and strip,” Korean Standards Association, Yeoksamdong, South Korea.
- KS F3021 (2013). “Structural glued laminated timber,” Korean Standards Association, Yeoksamdong, South Korea.
- Li, J., Rismanchi, B., and Ngo, T. (2019). “Feasibility study to estimate the environmental benefits of utilising timber to construct high-rise buildings in Australia,” *Building and Environment* 147, 108-120. DOI: 10.1016/j.buildenv.2018.09.052
- Loss, C., Piazza, M., and Zandonini, R. (2016a). “Connections for steel-timber hybrid prefabricated buildings. Part I: Experimental tests,” *Construction and Building Materials* 122, 781-795. DOI: 10.1016/j.conbuildmat.2015.12.002
- Loss, C., Piazza, M., and Zandonini, R. (2016b). “Connections for steel-timber hybrid prefabricated buildings. Part II: Innovative modular structures,” *Construction and Building Materials* 122, 796-808. DOI: 10.1016/j.conbuildmat.2015.12.001
- Metelli, G., Preti, M., and Giuriani, E. (2016). “On the delamination phenomenon in the repair of timber beams with steel plates,” *Construction and Building Materials* 102, 1018-1028. DOI: 10.1016/j.conbuildmat.2015.09.038
- Pang, S.-J., Ahn, K.-S., Jeong, S., Lee, G.-C., Kim, H. S., and Oh, J.-K. (2022). “Prediction of bending performance for a separable CLT-concrete composite slab connected by notch connectors,” *Journal of Building Engineering* 49, 103900. DOI: 10.1016/j.job.2021.103900
- Pang, S.-J., and Jeong, G. Y. (2018). “Load sharing and weakest lamina effects on the compressive resistance of cross-laminated timber under in-plane loading,” *Journal of Wood Science* 64(5), 538-550. DOI: 10.1007/s10086-018-1741-9
- Pang, S.-J., Lee, H.-J., Ahn, K.-S., and Oh, J.-K. (2020). “Sensitivity of censored data analysis to determine the characteristic value of structural timber,” *Journal of Wood Science* 66(1), 39. DOI: 10.1186/s10086-020-01885-0
- Pang, S.-J., Lee, H.-J., Yang, S. M., Kang, S. G., and Oh, J.-K. (2019). “Moment and shear capacity of Ply-lam composed with plywood and structural timber under out-of-plane bending,” *Journal of Wood Science* 65(1), 68. DOI: 10.1186/s10086-019-1847-8
- Pang, S.-J., Lee, J.-J., and Oh, J.-K. (2013). “Evaluation of allowable bending stress of dimension lumber; Confidence levels and size-adjustment,” *Journal of the Korean Wood Science and Technology* 41(5), 432-439. DOI: 10.5658/WOOD.2013.41.5.432
- Pang, S.-J., Oh, J.-K., Hong, J.-P., Lee, S.-J., and Lee, J.-J. (2018). “Stochastic model for predicting the bending strength of glued-laminated timber based on the knot area ratio and localized MOE in lamina,” *Journal of Wood Science* 64(2), 126-137. DOI: 10.1007/s10086-017-1682-8
- Pang, S.-J., Park, J.-S., Hwang, K.-H., Jeong, G.-Y., Park, M.-J., and Lee, J.-J. (2011). “Bending strength of Korean softwood species for 120×180 mm structural members,” *Journal of the Korean Wood Science and Technology* 39(5), 444-450. DOI: 10.5658/WOOD.2011.39.5.444
- Pang, S.-J., Shim, K.-B., and Kim, K.-H. (2021). “Effects of knot area ratio on the bending properties of cross-laminated timber made from Korean pine,” *Wood Science and Technology* 55(2), 489-503. DOI: 10.1007/s00226-020-01255-5
- Pang, S. J., and Jeong, G. Y. (2019). “Effects of combinations of lamina grade and thickness, and span-to-depth ratios on bending properties of cross-laminated timber (CLT) floor,” *Construction and Building Materials* 222, 142-151. DOI: 10.1016/J.CONBUILDMAT.2019.06.012
- Park, C.-Y., Pang, S.-J., Park, J.-S., Kim, K.-M., Park, M.-J., and Lee, J.-J. (2010). “Study of the distribution properties and LRFD code conversion in Japanese larch,” *Journal of the Korean Wood Science and Technology* 38(2), 94-100. DOI: 10.5658/WOOD.2010.38.2.94
- Petersen Raymer, A. K. (2006). “A comparison of avoided greenhouse gas emissions when using different kinds of wood energy,” *Biomass and Bioenergy* 30(7), 605-617. DOI: 10.1016/j.biombioe.2006.01.009
- Resch, E., Andresen, I., Cherubini, F., and Brattebø, H. (2021). “Estimating dynamic climate change effects of material use in buildings—Timing, uncertainty, and emission sources,” *Building and Environment* 187. DOI: 10.1016/j.buildenv.2020.107399
- Riola-Parada, F. (2016). *Timber-Steel Hybrid Beams for Multi-Storey Buildings*, Ph. D. Dissertation, Technische Universität Wien, Vienna, Austria. DOI: 10.34726/hss.2016.23820
- Röck, M., Saade, M. R. M., Balouktsi, M., Rasmussen, F. N., Birgisdottir, H., Frischknecht, R., Habert, G., Lützkendorf, T., and Passer, A. (2020). “Embodied GHG emissions of buildings - The hidden challenge for effective climate change mitigation,” *Applied Energy* 258. DOI: 10.1016/j.apenergy.2019.114107
- Sandanayake, M., Lokuge, W., Zhang, G., Setunge, S., and Thushar, Q. (2018). “Greenhouse gas emissions during timber and concrete building construction — A scenario based comparative case study,” *Sustainable Cities and Society* 38, 91-97. DOI: 10.1016/j.scs.2017.12.017
- Schober, K.-U., Harte, A. M., Kliger, R., Jockwer, R., Xu, Q., and Chen, J.-F. (2015). “FRP reinforcement of timber structures,” *Construction and Building Materials* 97, 106-118. DOI: 10.1016/j.conbuildmat.2015.06.020
- Tomasi, R., Parisi, M. A., and Piazza, M. (2009). “Ductile design of glued-laminated timber beams,” *Practice Periodical on Structural Design and Construction* 14(3), 113-122. DOI: 10.1061/(ASCE)1084-

- 0680(2009)14:3(113)
- Tsai, M.-T., and Le, T. (2018). "Determination of initial stiffness of timber-steel composite (TSC) beams based on experiment and simulation modeling," *Sustainability* 10(4), 1220. DOI: 10.3390/su10041220
- Wang, T., Wang, Y., Crocetti, R., Franco, L., Schweigler, M., and Wälinder, M. (2021). "An innovative timber-steel hybrid beam consisting of glulam mechanically reinforced by means of steel rod: Analytical and preliminary numerical investigations," *Journal of Building Engineering* 43, 102549. DOI: 10.1016/j.jobe.2021.102549
- Yan, H., Shen, Q., Fan, L. C. H., Wang, Y., and Zhang, L. (2010). "Greenhouse gas emissions in building construction: A case study of One Peking in Hong Kong," *Building and Environment* 45(4), 949-955. DOI: 10.1016/j.buildenv.2009.09.014